

## ac and dc percolative conductivity of magnetite-cellulose acetate composites

C. Chiteme,<sup>1,\*</sup> D. S. McLachlan,<sup>1,2</sup> and G. Sauti<sup>2</sup><sup>1</sup>Materials Physics Research Institute and School of Physics, University of the Witwatersrand, Private Bag 3, Wits 2050, South Africa<sup>2</sup>Department of Chemistry and Polymer Science, University of Stellenbosch, Private Bag XI, Matieland 7602, South Africa

(Received 23 November 2006; published 7 March 2007)

ac and dc conductivity results for a percolating system, which consists of a conducting powder (magnetite) combined with an “insulating” powder (cellulose acetate), are presented. Impedance and modulus spectra are obtained in a percolation system. The temperature dependence of the resistivity of the cellulose acetate is such that at 170 °C, it is essentially a conductor at frequencies below  $0.059 \pm 0.002$  Hz, and a dielectric above. The percolation parameters, from the dc conductivity measured at 25 and 170 °C, are determined and discussed in relation to the ac results. The experimental results scale as a function of composition, temperature, and frequency. An interesting result is the correlation observed between the scaling parameter ( $f_{ce}$ ), obtained from a scaling of the ac measurements, and the peak frequency ( $f_{cp}$ ) of the arcs, obtained from impedance spectra, above the critical volume fraction. Scaling at 170 °C is not as good as at 25 °C, probably indicating a breakdown in scaling at the higher temperature. The modulus plots show the presence of two materials: a conducting phase dominated by the cellulose acetate and the isolated conducting clusters below the critical volume fraction  $\phi_c$ , as well as the interconnected conducting clusters above  $\phi_c$ . These results are confirmed by computer simulations using the two exponent phenomenological percolation equation. These results emphasize the need to analyze ac conductivity results in terms of both impedance and modulus spectra in order to get more insight into the behavior of composite materials.

DOI: [10.1103/PhysRevB.75.094202](https://doi.org/10.1103/PhysRevB.75.094202)

PACS number(s): 72.80.Tm, 77.84.Lf, 81.05.Mh

## I. INTRODUCTION

The three standard percolation equations<sup>1,2</sup> have been used to describe the ac and dc conductivity of a large range of metal-insulator composites, as a function of volume fraction and frequency, for many years. However, recent studies have shown that one can use a single equation<sup>3-7</sup> that incorporates the three standard percolation equations as special cases. One crucial parameter is the critical volume fraction ( $\phi_c$ ), at which the conducting inclusions first form a spanning cluster, which is highly dependent on the very different microstructures.<sup>5,8-11</sup> The other two “structural” parameters are the exponents  $s$  and  $t$ .

In all previous experimental works (Refs. 1-7 and 9-12 and the references therein), the conducting phase had a conductivity so high that no impedance spectra could be measured, while the insulating phase had such a low conductivity that no impedance spectra could be obtained. In the present system, the temperature dependence of the conductivity of the insulating component [cellulose acetate (CA)] is such that impedance spectra could be measured above 120 °C. Magnetite is a sufficiently poor conductor that allows composite impedance spectra to be measured over the range 25-170 °C. The originality of these experiments is that, at 170 °C, the dc conductivity of the insulator is dominant at frequencies below 0.059 Hz, which enables full impedance and modulus arcs to be measured, both above and below ( $\phi_c$ ), in a percolation system.

The first results presented are the dc results, which are fitted to the two exponent phenomenological percolation equation (TEPPE) to obtain the all important dc percolation parameters. These dc results are then scaled as a function of temperature. ac scaling is presented next. Here, an interesting correlation is observed between the experimental scaling pa-

rameter ( $f_{ce}$ ), obtained from scaling of the measurements above the critical volume fraction onto a “master” curve, and the peak frequency ( $f_{cp}$ ) of the arcs, obtained from impedance spectra. Lastly, spectra for both the imaginary impedance  $Z''$  and modulus  $M''$  as a function of frequency are given and explained using the TEPPE. An interesting part is the detection of a separate contribution from the conducting clusters to the modulus spectra, below  $\phi_c$ , and a small contribution from the insulating component just above  $\phi_c$ .

## II. THEORETICAL BACKGROUND

The equations given in this section are perfectly general. However, the ideal limit of these equations does not necessarily apply to all the systems analyzed here. For all ac conductivity experiments, the composite conductivity ( $\sigma_m$ ) is the sum of the real and imaginary conductivities, which is given by  $\sigma_m = \sigma_{mr} + i\sigma_{mi}$ . The conductivity of the conducting component, magnetite ( $\text{Fe}_3\text{O}_4$ ) in this case, is given by  $\sigma_c = \sigma_{cr} + i\sigma_{ci}$  or simply  $\sigma_c = \sigma_{cr}$ , if ideal conductivity is assumed. For the insulating component, CA in this case, the conductivity is  $\sigma_i = \sigma_{ir} + i\sigma_{ii}$ , where  $\sigma_{ir} = \omega\epsilon_0\epsilon_{ir}$  (recall  $\omega = 2\pi f$ ). If ideal or lossless dielectric behavior is assumed,  $\sigma_i$  may be approximated as  $\sigma_i = i\omega\epsilon_0\epsilon_{ir}$  (i.e.,  $\sigma_{ir} = 0$ ). In practice,  $\sigma_{ir}$  incorporates both a usually very small dc conductivity [ $\sigma_{ir}(0)$ ] and the dielectric polarization loss term ( $\omega\epsilon_0\epsilon_{ii}$ ). In all previously reported ac percolation experiments,  $\sigma_{cr} \gg \omega\epsilon_0\epsilon_{cr}$  for the conducting component, and  $\sigma_{ir} \ll \omega\epsilon_0\epsilon_{ir}$  for the insulating component, which justified the assumption of ideal behavior for both the conductor and insulator.

In percolation theory, three regions must be distinguished: region I where  $\phi > \phi_c$ , region II where  $\phi < \phi_c$ , and region III, called the crossover region, where  $\phi \cong \phi_c$  and which lies between  $\phi - (\sigma_i/\sigma_c)^{1/(t+s)}$  [or  $(\omega\epsilon_0\epsilon_{ir}/\sigma_{cr})^{1/(t+s)}$ ] and  $\phi$

$+(\sigma_i/\sigma_c)^{1/(t+s)}$ . The expressions for the complex ac conductivity in these three regions for an ideal conductor and a lossless dielectric are<sup>1,2</sup>

$$\sigma_m = A\sigma_{cr}(\phi - \phi_c)^t - iB\omega\epsilon_0\epsilon_{ir}(\phi - \phi_c)^{-s} \text{ (region I),} \quad (1a)$$

$$\sigma_m = A'\omega\epsilon_0\epsilon_{ir}(\phi - \phi_c)^{-s} - B'\omega^2\epsilon_0^2\epsilon_{ir}^2/\sigma_{cr}(\phi_c - \phi)^{-t-2s} \text{ (region II),} \quad (1b)$$

$$\sigma_m = A''\sigma_{cr}^{s/(t+s)}(\omega\epsilon_0\epsilon_{ir})^{t/(s+t)} \text{ (region III).} \quad (1c)$$

Note that these equations are all power laws with arbitrary constants ( $A$ ,  $A'$ ,  $A''$ ,  $B$ , and  $B'$ ) and that there are no expressions for the regions between regions II and III as well as regions III and I.

In a recent series of papers,<sup>3-7,12-14</sup> it has been shown that the equation

$$(1 - \phi) \frac{\sigma_i^{1/s} - \sigma_m^{1/s}}{\sigma_i^{1/s} + A\sigma_m^{1/s}} + \phi \frac{\sigma_c^{1/t} - \sigma_m^{1/t}}{\sigma_c^{1/t} + A\sigma_m^{1/t}} = 0, \quad (2)$$

with  $A = (1 - \phi_c)/\phi_c$  and  $s$  and  $t$  as exponents, describes experimental results for percolation systems in a more exact and satisfactory manner, especially the second-order terms,<sup>6,7,13,14</sup> than Eqs. (1a)–(1c). When  $s = t = 1$ , the equation is equivalent to the Bruggeman symmetric media equation.<sup>5,9</sup> Equation (2) yields the two limits, when  $\sigma_i/\sigma_c$  is very small:

$$|\sigma_c| \rightarrow \infty: \sigma_m = \sigma_i \left( \frac{\phi_c}{\phi_c - \phi} \right)^s, \quad \phi < \phi_c, \quad (3)$$

$$|\sigma_i| \rightarrow 0: \sigma_m = \sigma_c \left( \frac{\phi - \phi_c}{1 - \phi_c} \right)^t, \quad \phi > \phi_c. \quad (4)$$

These equations are the normalized standard percolation equations<sup>1,2</sup> and characterize the exponents  $s$  and  $t$ . When  $\omega\epsilon_0\epsilon_{ir} \gg \sigma_{ir}$ , so that  $\sigma_i$  can be replaced by  $\omega\epsilon_0\epsilon_{ir}$  ( $= 2\pi f\epsilon_0\epsilon_{ir}$ ), Eq. (3) becomes

$$\epsilon_{mr} = \epsilon_{ir} \left( \frac{\phi_c}{\phi_c - \phi} \right)^s, \quad \phi < \phi_c. \quad (5)$$

This predicts a divergent  $\epsilon_{mr}$  as  $\phi$  approaches  $\phi_c$ .<sup>1,2</sup> In reality, for  $\phi > \phi_c$ ,  $\epsilon_{mr}$  (the second-order term for  $\phi > \phi_c$ ) shows a frequency and  $\phi$  dependent peak, above  $\phi_c$ .<sup>13,14</sup>

In the crossover region, Eq. (2) gives

$$\sigma_m \approx \sigma_i^{t/(s+t)} \sigma_c^{s/(s+t)} \text{ or } (2\pi f\epsilon_0\epsilon_{ir})^{t/(s+t)} \sigma_{cr}^{s/(s+t)}, \quad (6)$$

in agreement with Eq. (1c). In this region, for finite  $(\sigma_i/\sigma_c)$  the properties of both components have an effect on  $\sigma_m$ , which is not the case for the regions described by Eqs. (3) and (4). Note that Eq. (6) shows that in the crossover region, the conductivity ( $\sigma_{mr}$ ) is proportional to  $f^{t/(s+t)}$  and the dielectric constant  $\epsilon_{mr}$  (note that  $\epsilon_{xy} = \sigma_{xy}/2\pi f\epsilon_0$ ) is proportional to  $f^{s/(s+t)}$ . This is the same dispersion predicted by the standard percolation equations at higher frequencies for percolation systems close to  $\phi_c$ .<sup>1,2</sup> Note that within the crossover region, no disagreement, except for the arbitrary constant in the standard equations, between Eq. (2) and the

standard percolation equations has been observed experimentally, either in the first or second order.<sup>6,7</sup> However, it must again be emphasized that Eq. (2) can be used to fit experimental ac results, as a function of  $\phi$  and for all  $\phi$  and  $f$ , unlike Eqs. (1), (3), (4), and (6) which only apply in the restricted regions of  $\phi$  and  $f$ .

As scaling is used in this paper, the procedure is outlined here. The correct functions for two phase percolation systems, based on those given in Refs. 2 and 3 and outlined in Refs. 4 and 12, are

$$\sigma_m = \sigma_c \left( \frac{\phi_c - \phi}{\phi_c} \right)^t F_-(x_-), \quad \phi < \phi_c \quad (7a)$$

and

$$\sigma_m = \sigma_c \left( \frac{\phi - \phi_c}{1 - \phi_c} \right)^t F_+(x_+), \quad \phi > \phi_c, \quad (7b)$$

where  $\sigma_m$  can come from either theoretical calculations or experimental results. The scaling functions  $F_{\pm}(x_{\pm})$ , for ideal components, depend on the scaling parameters as follows:

$$x_- = \frac{f}{f_{c-}} = - \frac{2\pi f\epsilon_0\epsilon_{ir}}{\sigma_{cr}} \left( \frac{\phi_c - \phi}{\phi_c} \right)^{s+t}, \quad (8a)$$

$$x_+ = \frac{f}{f_{c+}} = - \frac{2\pi f\epsilon_0\epsilon_{ir}}{\sigma_{cr}} \left( \frac{1 - \phi_c}{\phi - \phi_c} \right)^{s+t}, \quad (8b)$$

or more generally,

$$x_- = \frac{[\sigma_i(0,0,T)](\phi_c - \phi)^{s+t}}{[\sigma_c(1,0,T)](\phi_c)^{s+t}}, \quad (8c)$$

$$x_+ = \frac{[\sigma_i(0,0,T)](1 - \phi_c)^{s+t}}{[\sigma_c(1,0,T)](\phi - \phi_c)^{s+t}}. \quad (8d)$$

Equation (8d) is used to scale the dc results as a function of temperature. Here,  $\sigma_{xy}$  is labeled to be a function of  $\phi$ ,  $f$ , and  $T$ .

The predictions for the slopes of the scaling functions  $\text{Re } F_+$ , which are obtained from scaling  $\sigma_{mr}$  above  $\phi_c$ , from standard percolation theory<sup>1,2</sup> and those obtained from Eq. (2) (Ref. 5 and 15) are the same. The previously defined crossover region now corresponds to  $f/f_{c+}$  and  $f/f_{c-} \approx 1$  as well as  $f/f_{c+}$  and  $f/f_{c-} > 1$ .

From Eq. (8b), the theoretical value of the critical frequency above  $\phi_c$  ( $f_{c+}$ ) is

$$f_{c+} = \frac{1}{2\pi} \frac{\sigma_c}{(\epsilon_0\epsilon_i)} \left( \frac{\phi - \phi_c}{1 - \phi_c} \right)^{s+t}. \quad (9)$$

A combination of Eqs. (7a) and (9) leads to a useful relation between the dc conductivity and  $f_{c+}$ :

$$f_{c_+} \propto \sigma_m(\phi, 0)^{(s+i)/q} [\equiv \sigma_m(\phi, 0)^q]. \quad (10)$$

Note that in this paper, as well as in previous works<sup>1,2</sup> for ac results,  $f_{c_+}$  is calculated using a purely real  $\sigma_c(\sigma_{ci}=0)$  and purely imaginary  $\sigma_i(\sigma_{ir}=0)$ . Although this may not be strictly true in the present experiments, the experimental results are scaled using this well established procedure.

Cole-Cole plots (imaginary impedance against real impedance and imaginary modulus against real modulus) are useful in the impedance spectroscopy study of multiphase systems.<sup>16</sup> However, it is often more instructive to plot  $Z''(f)$  and  $M''(f)$ . For binary (two phase) systems, Cole-Cole,  $Z''(f)$ , and  $M''(f)$  plots of the results for a percolation system below  $\phi_c$  will, if similar to some effective media systems, show two arcs,<sup>17</sup> each corresponding to one of the phases. This enables both a characteristic or peak frequency ( $f_p$ ) for each of the components to be measured.

In order that two arcs appear in Cole-Cole,  $Z''(f)$ , and  $M''(f)$  plots, the characteristic frequency of each of the components must be within the experimental frequency range and the microstructure of the composite must lead to measurable values of impedance or modulus. In previous percolation experiments, the impedance arc of both insulating and conducting components was either neglected or, more often, could not be measured by the available instrumentation. Therefore, impedance spectra for percolation systems have not been previously presented. If similar to most effective media systems, spectra above  $\phi_c$  should show only a single arc, the peak frequency of which is determined by the properties of the components and the volume fraction of each.<sup>17</sup> The peak frequencies for the multiple component arc (above  $\phi_c$ ) or the two single composite arcs (below  $\phi_c$ ) are given by

$$f_p = \frac{\sigma_{mr}(0)}{2\pi\epsilon_0\epsilon_{mr}(0)} \quad (\phi > \phi_c), \quad (11a)$$

$$f_p = \frac{\sigma_{cr}(0)}{2\pi\epsilon_0\epsilon_{cr}(0)} \quad (\phi < \phi_c, \text{ high frequency}), \quad (11b)$$

$$f_p = \frac{\sigma_{ir}(0)}{2\pi\epsilon_0\epsilon_{ir}(0)} \quad (\phi < \phi_c, \text{ low frequency}), \quad (11c)$$

respectively. The subscript ‘‘m’’ refers to the property of the composite and ‘‘c’’ and ‘‘i’’ to the components. The  $\sigma_{xr}(0)$  and  $\epsilon_{xr}(0)$  are the dc conductivities and static dielectric constants, respectively. In some solid electrolyte systems (Ref. 18 and the references therein), it has been observed that the use of both complex impedance ( $Z^*$ ) and modulus ( $M^*$ ) representations provides a better understanding of the relaxation properties of the investigated material. In this paper, both representations are needed to understand the results obtained. The notations adopted for  $Z^*$  and  $M^*$  are  $Z^* = Z' - iZ''$  and  $M^* = M' + iM''$ . Here,  $Z'$  ( $M'$ ) and  $Z''$  ( $M''$ ) are the real and imaginary impedances (moduli), respectively.  $M^* = i2\pi fZ^*$ , which leads to the following equations:

$$M' = 2\pi fZ'' \quad (12a)$$

and

$$M'' = 2\pi fZ'. \quad (12b)$$

Note, from both simulations and experiments, that  $Z''/Z'$  and  $Z''$  versus  $f$  plots give single arcs for all values of  $\phi$ . Above  $\phi_c$ , the peak frequency ( $f_p$ ) increases with  $\phi$ . The experimental  $M''-M'$  and  $M''$  versus  $f$  plots are more complex, but can be semiquantitatively fitted using Eq. (2) with a dispersive expression for properties of the CA. These results will be given in the experimental section to confirm these unexpected observations.

### III. EXPERIMENTAL PROCEDURE

The CA powder was heated overnight in an oven at 150 °C to remove moisture. The dry powder was then weighed and mixed with a predetermined mass of Fe<sub>3</sub>O<sub>4</sub> powder in a small bottle, which was then tumbled for 10 min. 2.50 to 3.00 g of the mixture was then compressed into pellets at 380 MPa. The pressure was maintained at this value for about one and a half hours.

The mass and volume of the pellet were then measured to determine the porosity prior to annealing at 180 °C for 12 h. The annealing step was necessary in order to have a stable system at 170 °C, as it had previously been established that the cellulose acetate first gave a complete impedance arc on a Cole-Cole plot at the 170 °C temperature. The mass and volume of the pellet were then measured again and these parameters were used to determine the volume fraction of the conducting component (Fe<sub>3</sub>O<sub>4</sub>), the porosity being included in the insulator volume fraction when calculations were made. This procedure was used to prepare a series of samples spanning both the insulating and conducting regions (i.e., below and above  $\phi_c$ ).

In a previous work,<sup>12</sup> samples were made by mixing the same Fe<sub>3</sub>O<sub>4</sub> with approximately 300 μm talc wax particles and compressing the mixture together. The macrostructure was very different from the present samples, but the microstructure of the Fe<sub>3</sub>O<sub>4</sub> component was probably similar. Some results for this system are presented for comparison.

Prior to conductivity measurements, electrodes were painted onto the samples using colloidal silver paint. The dc conductivity measurements were made using a Keithley 617 electrometer configured in the  $V/I$  mode, while ac conductivity measurements were done on a Novocontrol Broadband Dielectric Converter, operated within a frequency range of 10<sup>-2</sup>–3 × 10<sup>6</sup> Hz. Detailed dc and ac measurements were made at room temperature (25 °C) and 170 °C in a small custom made oven. Further ac measurements were made at 40, 60, 80, 100, 120, 140, and 160 °C. The results were then plotted in various forms for further analysis and interpretation.

### IV. RESULTS AND DISCUSSION

Note that a great deal of the discussion related to Fig. 8 onward is in terms of the theoretical  $f_{c_+}$  or  $f_{c_1}$  [Eq. (9)] and the experimental  $f_{ce}$  and  $f_{cp}$ . The measurement of  $f_{ce}$  is outlined later in the text as is that of  $f_{cp}$ .

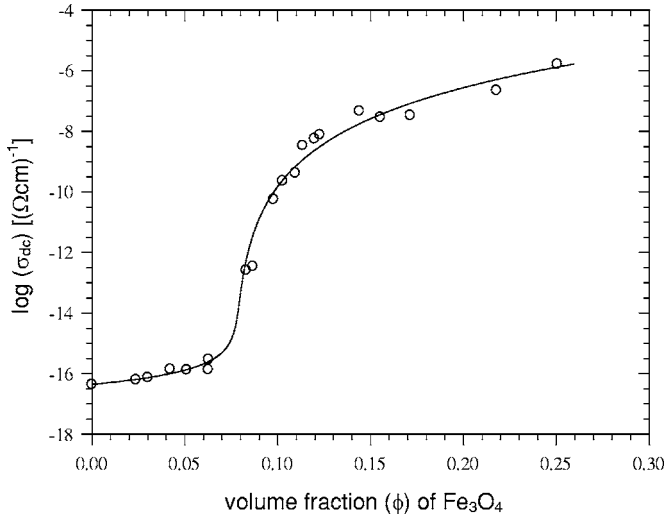


FIG. 1. dc results for the  $\text{Fe}_3\text{O}_4$  in cellulose acetate system at 25 °C.

Figures 1 and 2 show the dc experimental results as the log of the conductivity  $[\sigma_{mr}(\phi, 0)]$  plotted against the magnetite ( $\text{Fe}_3\text{O}_4$ ) volume fraction ( $\phi$ ) at 25 and 170 °C, respectively. The continuous lines are best fits to Eq. (2). The best-fit parameters at 25 °C are  $\log(\sigma_{cr}) = -2.57 \pm 0.46$ ,  $\log(\sigma_{ir}) = -16.36 \pm 0.06$ ,  $\phi_c = 0.076 \pm 0.009$ ,  $s = 1.03 \pm 0.32$ , and  $t = 4.57 \pm 0.65$ , while the corresponding parameters at 170 °C are  $\log(\sigma_{cr}) = -0.123 \pm 0.53$ ,  $\log(\sigma_{ir}) = -12.93 \pm 0.09$ ,  $\phi_c = 0.074 \pm 0.021$ ,  $s = 1.30 \pm 0.53$ , and  $t = 5.94 \pm 0.71$  (Table I). All  $\sigma$  values are in  $(\Omega \text{ cm})^{-1}$ . Note that the  $\phi_c$  values at the two temperatures agree within experimental error, which indicates that the microstructure remains the same. However, the  $\text{Fe}_3\text{O}_4$  interparticle conductances almost certainly change with temperature, as the pressure on the contact points will change with temperature due to differences in the thermal expansion of the two components. The  $\phi_c$  value is typical of a composite made from grains of roughly equal size but with the conducting powder diameter being a little smaller than that of the insulating component. Here, a value somewhat below 0.16 is expected.<sup>8,12</sup> While the scatter of the points at

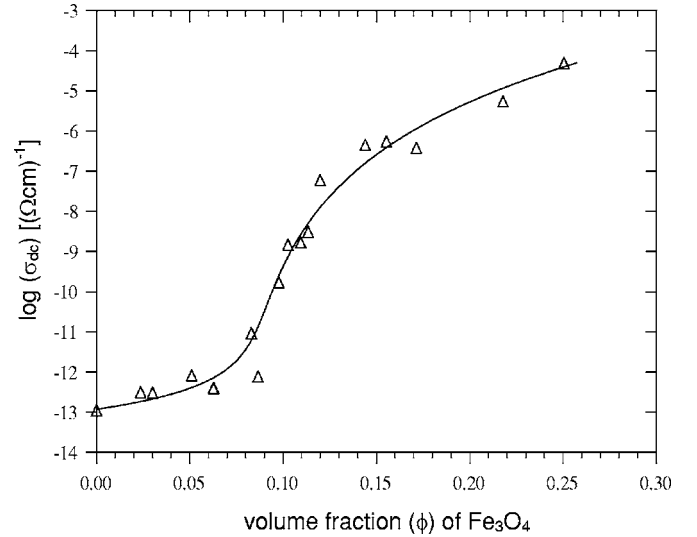


FIG. 2. dc results for the  $\text{Fe}_3\text{O}_4$  in cellulose acetate system at 170 °C.

170 °C is larger, the pattern of the deviations at both temperatures is similar. The crossover region,  $\phi_c \pm (\sigma_i/\sigma_c)^{1/(s+t)}$ , lies between 0.070 and 0.082 at 25 °C and does not include any experimental points. At 170 °C, the same region extends from 0.046 to 0.102 and includes six or seven points. These results, together with those for  $\text{Fe}_3\text{O}_4$ -talc wax<sup>12</sup> which are given for comparison, are summarized in Table I.

A comparison of the  $s$  and  $t$  exponents at the two temperatures shows that the corresponding exponents at 170 °C are marginally higher than those at 25 °C, indicating that there may be a weak temperature dependence of the exponents. Note, too, that the conductivity ratio  $(\sigma_{ir}/\sigma_{cr})$  at 25 °C is a factor of 10 smaller than that at 170 °C. The dependence of exponent  $t$  on the conductivity ratio has been observed (albeit in the opposite direction) in a cellular system.<sup>12</sup> In Ref. 12,  $t$  was found to decrease with increasing  $\sigma_{ir}/\sigma_{cr}$  in the magnetite-talc wax system, whereas in the present systems,  $t$  is observed to increase (refer to Table I). The reason for this difference in behavior is not clear. However, in the present case the higher temperature may give rise

TABLE I. Measured and calculated percolation parameters for the FeCA and FeTW systems.

Parameter	FeCA (25 °C)	FeTW (25 °C)	FeCA (170 °C)
$\phi_c$	$0.076 \pm 0.009$	$0.025 \pm 0.003$	$0.074 \pm 0.021$
$s$	$1.03 \pm 0.32$	$0.45 \pm 0.31$	$1.30 \pm 0.53$
$t$	$4.57 \pm 0.65$	$4.12 \pm 0.23$	$5.94 \pm 1.71$
$\sigma_{cr} [(\Omega \text{ cm})^{-1}]$	$(2.69 \pm 0.48) \times 10^{-3}$	$(2.63 \pm 0.48) \times 10^{-3}$	$(0.75 \pm 0.08)$
$\sigma_{ir} [(\Omega \text{ cm})^{-1}]$	$(4.36 \pm 0.02) \times 10^{-17}$	$(8.51 \pm 0.48) \times 10^{-16}$	$(1.17 \pm 0.01) \times 10^{-13}$
$\sigma_{ir}/\sigma_{cr}$	$1.62 \times 10^{-14}$	$3.24 \times 10^{-13}$	$1.56 \times 10^{-13}$
$(\sigma_{ir}/\sigma_{cr})^{1/(t+s)}$	$3.45 \times 10^{-3}$	$1.85 \times 10^{-3}$	$1.70 \times 10^{-2}$
$u_e$	$0.754 \pm 0.007$	$0.73 \pm 0.01$	$0.831 \pm 0.008$
$u_t$	$0.82 \pm 0.28$	$0.90 \pm 0.67$	$0.82 \pm 0.41$
$q_{ce}$	$1.10 \pm 0.17$	$1.06 \pm 0.04$	$1.05 \pm 0.10$
$q_{cp}$	$1.10 \pm 0.17$	$1.10 \pm 0.17$	$1.00 \pm 0.08$
$q_{ct}$	$1.225 \pm 0.002$	$1.11 \pm 0.18$	$1.31 \pm 0.16$

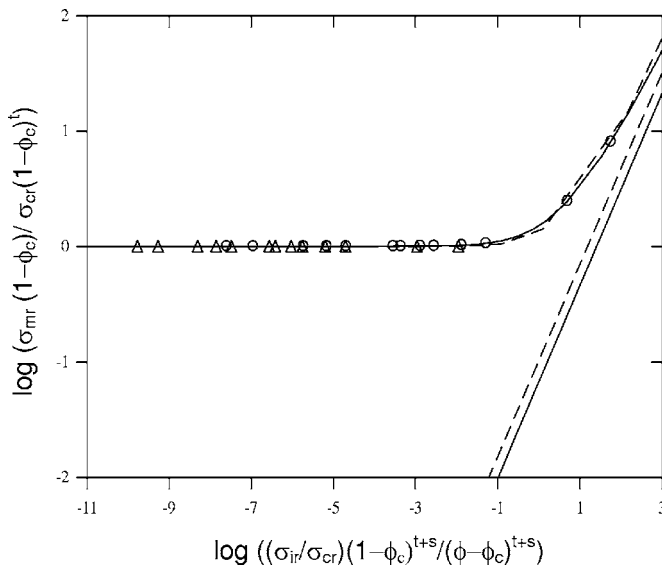


FIG. 3. Scaled dc results for  $\text{Fe}_3\text{O}_4$  in cellulose acetate system at 25 °C ( $\Delta$ ) and 170 °C ( $\circ$ ).

to a larger range of interparticle resistance which will give a higher  $t$  value.<sup>19</sup> The  $t$  values are, if the experimental error is taken into account, only a little larger than those observed in a magnetite-talc wax system (Refs. 12 and 20 and the references therein). (In the cellular system where the conducting grains are 30 times smaller than the insulating grains, this leads to a  $\phi_c$  value of  $0.025 \pm 0.003$ .<sup>8</sup>) Note that the high  $t$  value observed in the present system is in the same high  $t$  range as those in Ref. 12, which were attributed to the presence of a large range of interparticle conductance<sup>19</sup> arising from the hard and highly angular magnetite and niobium carbide grains.<sup>12</sup> However, the  $s$  values are considerably larger than the value of  $0.45 \pm 0.31$  observed in the cellular (magnetite-talc wax) system. This high value of  $s$  appears to contradict the observation in Ref. 12 that the hard and angular conductors (magnetite and niobium carbide) in the cellular systems<sup>8,12</sup> have very low  $s$  values associated with the high  $t$  values. This observation again highlights the fact that the current knowledge regarding  $t$  values is inadequate and that there is no theory of the observed  $s$  values in this and all other static percolation systems. [Note that larger  $s$  values are predicted for dynamic percolation systems<sup>21</sup> (e.g., oil-water emulsions) and also for static two-dimensional systems, where  $s=t$ .] From the above, one can conclude that the system made from a poor conductor and a poor insulator does not have an effect on the dc percolation properties, which are still best described by Eq. (2).

In Fig. 3, the dc scaling of the results at 25 and 170 °C, using Eqs. (7b) and (8d), is illustrated. As shown in Table I, the ratio  $\sigma_{ir}/\sigma_{cr}$  increases by only a factor of 10 from 25 to 170 °C due to the fact that both  $\sigma_{ir}$  and  $\sigma_{cr}$  increase with temperature. Despite this, the experimental points move sufficiently along the scaling curves generated by Eq. (2) to illustrate its validity. Recall that none of the samples lie in the crossover region at 25 °C, but there are several in this region at 170 °C. The only other previous plot of this nature is given in Ref. 12, where it was also shown that the dc

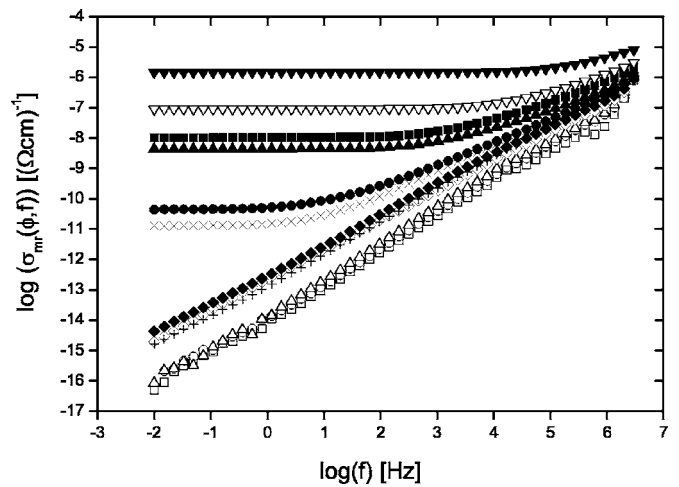


FIG. 4. ac conductivity results for the  $\text{Fe}_3\text{O}_4$  in cellulose acetate system at 25 °C.  $\phi=0.0000$  ( $\square$ ), 0.0237 ( $\circ$ ), 0.0421 ( $\Delta$ ), 0.0510 ( $\diamond$ ), 0.0628 ( $+$ ), 0.0830 ( $\blacklozenge$ ), 0.0977 ( $\times$ ), 0.1026 ( $\bullet$ ), 0.1198 ( $\blacktriangle$ ), 0.1440 ( $\blacksquare$ ), 0.2178 ( $\nabla$ ), and 0.2505 ( $\blacktriangledown$ ).

exponent  $t$  decreased with increasing  $\sigma_{ir}/\sigma_{cr}$ . The slight difference or separation in the theoretical curves in Fig. 3 is a result of the difference in the  $t$  exponents at the two temperatures. It must be emphasized that standard percolation theory does not give an analytic or scaling expression in the region of  $f/f_{ct}$  or  $f/f_{ce} \sim 1$ . The fact that this scaling is achieved using the previously measured dc parameters means that, for dc scaling, the system is “universal.” Fitting the experimentally scaled ac results using the exact same dc parameters has never proved to be possible (this paper and Refs. 4 and 12). This is addressed in detail in Ref. 22.

Figures 4 and 5 show the ac experimental results plotted as the logarithm of the real conductivity against the logarithm of the frequency in the range  $10^{-2} - 3 \times 10^6$  Hz at 25 and 170 °C, respectively. The results at 25 °C show the familiar pattern (Refs. 4, 12, and 14 and the references therein) with the conductivity below  $\phi_c$  being dominated by the di-

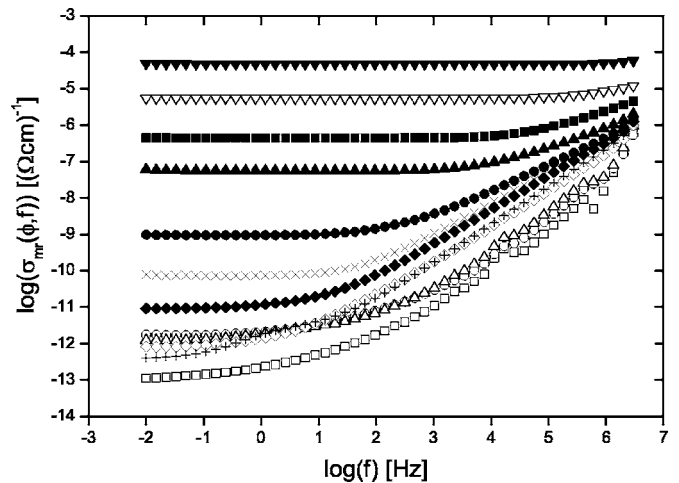


FIG. 5. ac conductivity results for the  $\text{Fe}_3\text{O}_4$  in cellulose acetate system at 170 °C.  $\phi=0.0000$  ( $\square$ ), 0.0237 ( $\circ$ ), 0.0421 ( $\Delta$ ), 0.0510 ( $\diamond$ ), 0.0628 ( $+$ ), 0.0830 ( $\blacklozenge$ ), 0.0977 ( $\times$ ), 0.1026 ( $\bullet$ ), 0.1198 ( $\blacktriangle$ ), 0.1440 ( $\blacksquare$ ), 0.2178 ( $\nabla$ ), and 0.2505 ( $\blacktriangledown$ ).

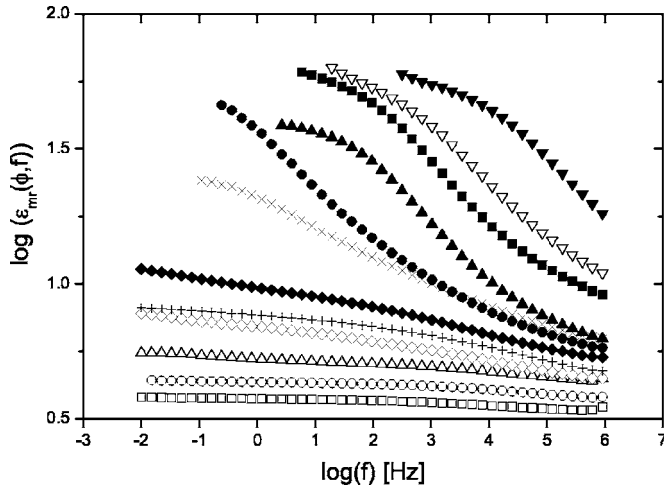


FIG. 6. Dielectric constant results for the  $\text{Fe}_3\text{O}_4$  in cellulose acetate system at  $25^\circ\text{C}$   $\phi=0.0000$  ( $\square$ ),  $0.0237$  ( $\circ$ ),  $0.0421$  ( $\triangle$ ),  $0.0510$  ( $\diamond$ ),  $0.0628$  ( $+$ ),  $0.0830$  ( $\blacklozenge$ ),  $0.0977$  ( $\times$ ),  $0.1026$  ( $\bullet$ ),  $0.1198$  ( $\blacktriangle$ ),  $0.1440$  ( $\blacksquare$ ),  $0.2178$  ( $\nabla$ ), and  $0.2505$  ( $\blacktriangledown$ ).

electric loss of the cellulose acetate, which increases in accordance with Eq. (2). The low  $\phi$  expansion of Eq. (2)  $\{\epsilon_m = \epsilon[1 + (s\phi/\phi_c)]\}$  is given in Ref. 14. This paper (Ref. 14) also discusses how, except for extremely low loss dielectrics, the loss or conductivity due to the percolation clusters is not observable below  $\phi_c$ . Cellulose acetate is an unusual dielectric in that the dispersion coefficient  $x(\sigma = C\omega^x)$  of its conductivity (dielectric loss) is closer to 1.1 than the commonly observed values, which tend to be close to 0.9.<sup>23</sup> The limiting slope, for low  $|\phi - \phi_c|$  and high frequency, is predicted to be  $t/(s+t)$  both just above and just below  $\phi_c$  by Eqs. (1c), (2), and (10). The decrease in the slope of  $\sigma_{mr}$  for small  $|\phi_c - \phi|$  and high frequencies to less than 1 [i.e.,  $t/(s+t)$ ] is clearly seen in Fig. 4 as well as in Refs. 4 and 12.

The results at  $170^\circ\text{C}$  do not follow previously observed trends. The effects of the increased dc conductivity of the CA can clearly be seen below  $\phi_c$  since for frequencies less than 1 Hz (see later), the dielectric loss approaches the dc conductivity and the slope is nearly frequency independent. The slope observed in Fig. 5, below  $\phi_c$  and at higher frequencies, is just greater than 1. The reason why the characteristic decrease in the slope for low  $|\phi - \phi_c|$  at high frequency, as seen in Fig. 4 and predicted by percolation theory for ideal systems, is not observed is that this is a far from ideal case (i.e.,  $\sigma_{ir}/\sigma_{cr}$  is not very small). While the conductivity plots above  $\phi_c$  have the usual shape, the frequency ( $f_{ce}$ ) at which the curves turn up is higher than that at  $25^\circ\text{C}$ , in accord with Eq. (9). Note, too, that due to the high dc conductivity in the cellulose acetate, one can no longer easily differentiate between samples above and below  $\phi_c$  from a plot of this nature.

Figures 6 and 7 show the results for the logarithm of the real dielectric constant ( $\epsilon_{mr}$ ) plotted against the logarithm of the frequency at  $25$  and  $170^\circ\text{C}$ , respectively. The graphs both show that as  $\phi_c$  is approached from below, the dielectric constant is enhanced at all frequencies but the dielectric enhancement [Eq. (5)] or  $s$  is decreasing with frequency as previously seen in Ref. 12. Closer to  $\phi_c$ , the dielectric con-

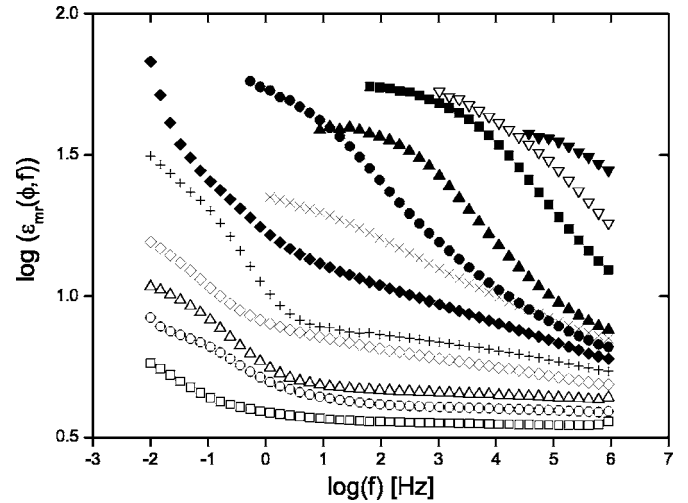


FIG. 7. Dielectric constant results for the  $\text{Fe}_3\text{O}_4$  in cellulose acetate system at  $170^\circ\text{C}$   $\phi=0.0000$  ( $\square$ ),  $0.0237$  ( $\circ$ ),  $0.0421$  ( $\triangle$ ),  $0.0510$  ( $\diamond$ ),  $0.0628$  ( $+$ ),  $0.0830$  ( $\blacklozenge$ ),  $0.0977$  ( $\times$ ),  $0.1026$  ( $\bullet$ ),  $0.1198$  ( $\blacktriangle$ ),  $0.1440$  ( $\blacksquare$ ),  $0.2178$  ( $\nabla$ ), and  $0.2505$  ( $\blacktriangledown$ ).

stant is both enhanced and has increasing negative dispersion [from Eq. (5)]. This pattern is continued up until  $\phi = 0.0866$  ( $\phi > \phi_c$ ), but the curves become more complex for still higher  $\phi$  values. The shape of these curves is in qualitative agreement with what is observed in some other systems.<sup>4,13,14</sup> The anomalous behavior of the second-order real dielectric constant above  $\phi_c$  is examined in more detail in Refs. 13 and 14, where it is shown to be in accord with Eq. (2) and in disagreement with the standard percolation equations. The increase in the measured  $\epsilon_{mr}$  at low frequencies ( $< 1$  Hz) that is observed at  $170^\circ\text{C}$  for low  $\phi$  values is primarily due to the cellulose acetate, as is also observed in the  $\phi=0.0000$  sample at  $170^\circ\text{C}$ . It will later be shown that

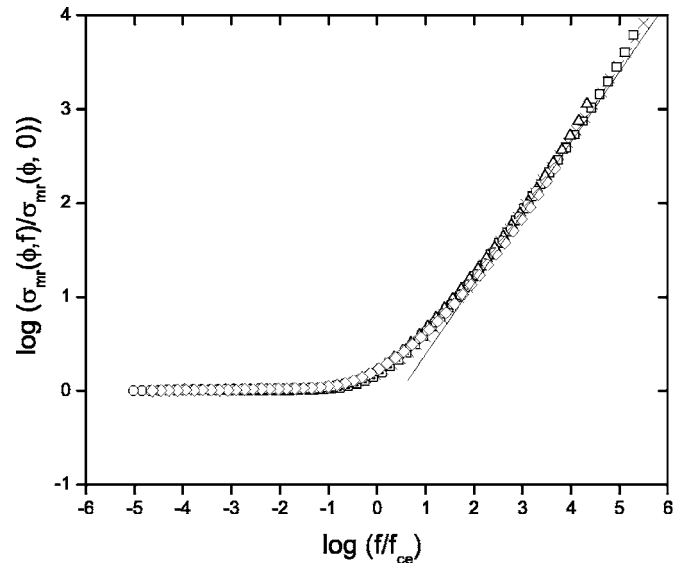


FIG. 8. ac conductivity results above  $\phi_c$  for the  $\text{Fe}_3\text{O}_4$  in cellulose acetate system at  $25^\circ\text{C}$  scaled by  $1/f_{ce}$  for  $\phi=0.1026$  ( $\times$ ),  $0.1094$  ( $\square$ ),  $0.1134$  ( $\triangle$ ),  $0.1440$  ( $\circ$ ), and  $0.1553$  ( $\diamond$ ). The solid line is a linear fit to the data, which gives a slope ( $u_c$ ) of  $0.754 \pm 0.007$ .

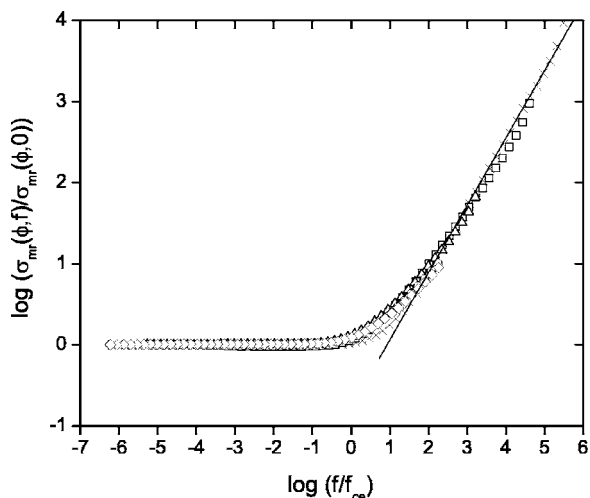


FIG. 9. ac conductivity results above  $\phi_c$  for the  $\text{Fe}_3\text{O}_4$  in cellulose acetate system at 170 °C scaled by  $1/f_{ce}$  for  $\phi=0.1026$  ( $\times$ ), 0.1094 ( $\square$ ), 0.1134 ( $\triangle$ ), 0.1440 ( $\circ$ ), and 0.1553 ( $\diamond$ ). The solid line is a linear fit to the data, which gives a slope ( $u_e$ ) of  $0.831 \pm 0.008$ .

cellulose acetate is essentially a conductor at these low frequencies.

Figures 8 and 9 show the results of scaling the experimental conductivity results above  $\phi_c$ , given as a plot of the  $\log(\sigma_{mr}(\phi, f)/\sigma_{mr}(\phi, 0))$  against  $\log(f/f_{ce})$  at 25 and 170 °C, respectively. In both cases, the conductivity results are first divided by the dc or low-frequency conductivity and the resulting curves are then slid along the  $\sigma_{mr}(\phi, f)/\sigma_{mr}(\phi, 0)=0$  line until the linear regions give the best overlap. This involves sliding the normalized curves along the  $\log(f)$  axis by a factor of  $\log(1/f_{ce})$  and determines the experimental values of  $f_{ce}$ , which are given in Table II. It can be seen that at 25 °C the curves all scale onto each other and the limiting slope ( $u_e$  in Table I) is found to be  $0.754 \pm 0.007$ . The results at 170 °C also scale, but cannot be made to overlap as closely as those at 25 °C, indicating a

TABLE II. Measured and calculated  $f_{cp}$ ,  $f_{ce}$ , and  $f_{ct}$  parameters for the FeCA and FeTW systems.

System	$\phi$	$f_{cp}$ (Hz)	$f_{ce}$ (Hz)	$f_{ct}$ (Hz)
FeCA (25 °C)	0.1026	3.417	4.30	3.14
	0.1094	4.432	10.50	11.22
	0.1134	93.562	93.56	21.15
	0.1440	1333.21	1059.00	601.52
FeCA (170 °C)	0.1026	55.16	98.08	0.04
	0.1094	74.58	296.89	0.21
	0.1134	1862.09	4677.36	0.45
	0.1440	17096.22	54063.89	28.76
FeTW (25 °C)	0.0486	27.74	100	27.81
	0.0602	159.59	724.44	172.85
	0.0823	2040.80	10000.00	1602.32
	0.1088	10244.72	39810.72	9103.50

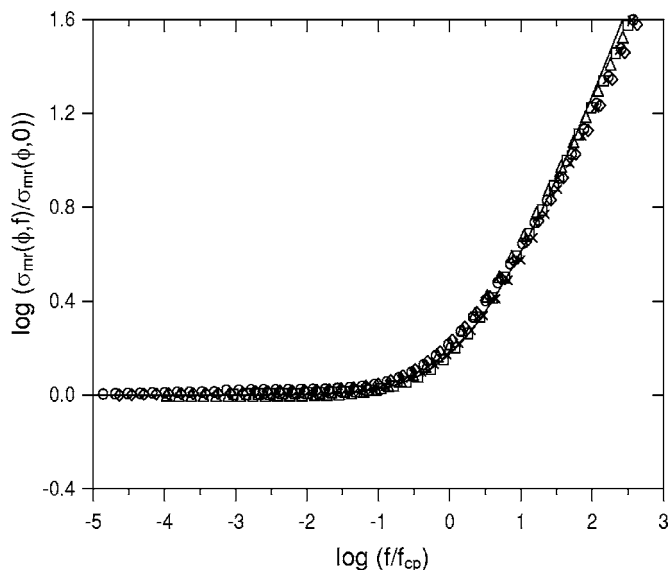


FIG. 10. ac conductivity results for the  $\text{Fe}_3\text{O}_4$  in cellulose acetate system at 25 °C scaled by  $1/f_{cp}$  and superimposed onto the dc curve. Samples [ $\phi=0.1026$  ( $\times$ ), 0.1094 ( $\square$ ), 0.1134 ( $\triangle$ ), 0.1440 ( $\circ$ ), and 0.1553 ( $\diamond$ )] are above  $\phi_c$ .

breakdown in scaling due to a conductive dielectric insulator. The best-fit limiting slope is  $0.831 \pm 0.008$ . At 25 and 170 °C, the corresponding theoretical values of  $u_t=t/(s+t)$ , obtained using the measured dc parameters, are  $0.82 \pm 0.28$  and  $0.82 \pm 0.41$ , respectively. Note also that the value of  $u_e$ , at 170 °C, is very close to that obtained in the magnetite cellular system,<sup>12</sup> while the present  $u_t$  is smaller than the one from the cellular system, probably because of the smaller  $s$  measured there. The results for the various  $u$  values are summarized in Table I. Note that correct universal behavior requires better agreement between the theoretical value of  $u$  and the experimental value.

It should also be noted that in Fig. 9, at 170 °C, the best scaling of the experimental results using the values of  $f_{ce}$  obtained by “sliding” (which does not depend on any particular theory) results in a thickening of the overlap of the results in the  $f/f_{ce}=1$  region. This is due to the best overlap in the linear slope criterion.

Figures 10 and 11 show plots of the experimental results for  $\log(\sigma_{mr}(\phi, f)/\sigma_{mr}(\phi, 0))$  against  $\log(f/f_{cp})$  at 25 and 170 °C, respectively. Superimposed on these results is the previously defined scaling curve, obtained from Eq. (2), using the dc parameters obtained at 25 and 170 °C. The  $f_{cp}$ 's in these plots (see Table II) are obtained from the  $Z''(f)$  plots given later; therefore, there are no new phenomenologically determined parameters, such as  $f_{ce}$ , used in these plots. The superposition at 25 °C is very good, which shows that scaling can be achieved using  $f_{cp}$  values obtained from  $Z''(f)$  arcs. The experimental results for  $\phi=0.1026$  and 0.1094 at 170 °C in Fig. 11 deviate from each other in the lower-frequency  $f/f_{cp}=1$  region, and more seriously at higher frequency, indicating a serious breakdown of “ideal” scaling due to a nonideal dielectric insulator. The  $\phi=0.1134$ , 0.1440, and 0.1553 results show moderate agreement with the theoretical curve obtained using the dc parameters. This, com-

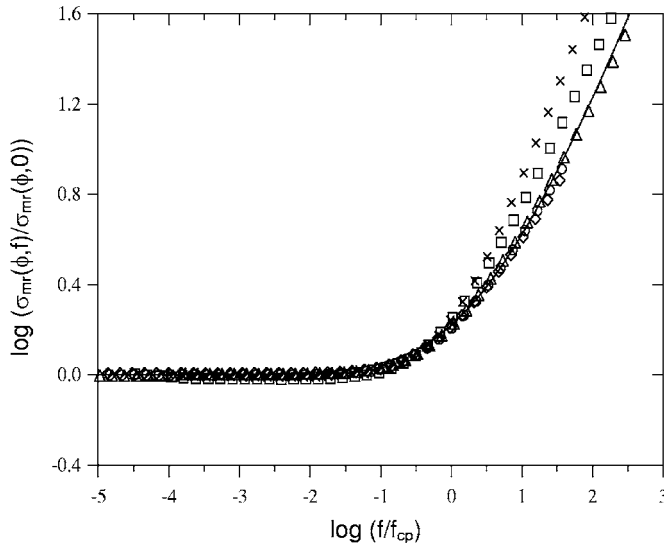


FIG. 11. ac conductivity results for the  $\text{Fe}_3\text{O}_4$  in cellulose acetate system at  $170^\circ\text{C}$  scaled by  $1/f_{cp}$  and superimposed onto the dc curve. Samples [ $\phi=0.1026$  ( $\times$ ),  $0.1094$  ( $\square$ ),  $0.1134$  ( $\triangle$ ),  $0.1440$  ( $\circ$ ), and  $0.1553$  ( $\diamond$ )] are above  $\phi_c$ .

bin with the remarks made with regard to Figs. 8 and 9, makes it clear that there is a breakdown of scaling when the dielectric insulator starts to show conducting properties.

To test Eq. (10), plots (not shown) of  $\log(f_{cp})$  (the impedance arc peak frequency, see later) against the  $\log(\text{dc conductivity})$  [ $\equiv \log(\sigma_{mr}(\phi, 0))$ ], above  $\phi_c$ , at  $25$  and  $170^\circ\text{C}$  were made. These resulted in linear plots, from which the slope  $q_{cp}$  [Eq. (10)] is found to be  $1.10 \pm 0.17$  and  $1.00 \pm 0.08$ , respectively. From Table I, it can be seen that these values of the slopes are in good agreement with  $q_{ce}$  and the previous result for magnetite powder in the cellular system,<sup>12</sup> but somewhat lower than  $q_{ct}=(s+t)/t$ . Recall that  $f_{cp}$  above  $\phi_c$  is a property of the composite and not the individual components.

Plots were also made of  $\log(f_{ce})$  against the dc conductivity at  $25$  and  $170^\circ\text{C}$ . As expected, the results give linear plots, in agreement with Eq. (10). The corresponding  $q_{ce}$  exponents are  $1.10 \pm 0.17$  and  $1.05 \pm 0.10$ , respectively, in close agreement with those obtained using  $f_{cp}$ . Table II indicates that at the lower temperature ( $25^\circ\text{C}$ ),  $f_{cp} \approx f_{ce}$ . Theory shows that this should be so, as can be seen by substituting Eq. (4) into Eq. (9) to obtain Eq. (11).

The theoretical values of  $f_{ct}$  [calculated from Eq. (9) using the dc parameters], given in Table II, were also plotted against the experimental dc conductivity [ $\sigma_{mr}(\phi, 0)$ ] at  $25$  and  $170^\circ\text{C}$ . The exponents  $q_{ct}$  obtained from these linear plots are found to be  $1.225 \pm 0.002$  and  $1.31 \pm 0.16$ , respectively (Table I). These calculated  $q_{ct}$  exponents are close to but higher than the measured values  $q_{ce}$  and  $q_{cp}$ . While Tables I and II show that the  $q_{ce}$ ,  $q_{cp}$  and  $f_{ce}$ ,  $f_{cp}$  values are reasonably close at  $25^\circ\text{C}$ , these values differ widely at  $170^\circ\text{C}$ . These observations indicate that for the system studied here,  $f_{ce}$  is closer to the value of  $f_{cp}$  than the  $f_{ct}$  value calculated from the scaling theory. These results go further to illustrate some shortcomings or the breakdown in the theory regarding the critical frequencies, especially at  $170^\circ\text{C}$ , de-

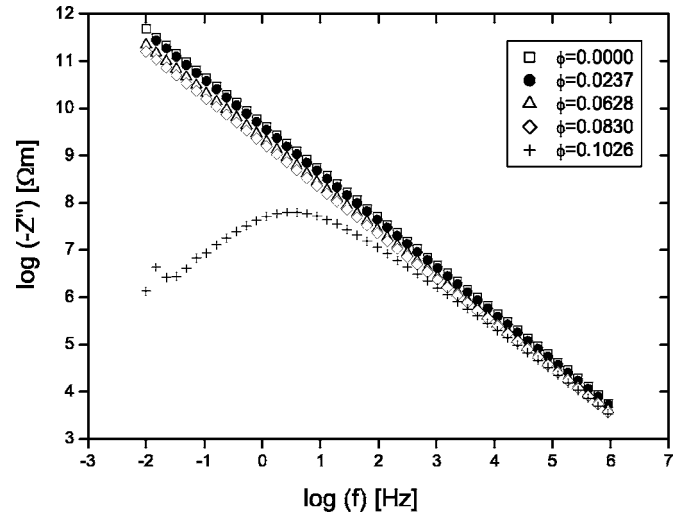


FIG. 12. Logarithm of imaginary impedance results plotted against logarithm of frequency for various samples of the  $\text{Fe}_3\text{O}_4$  in cellulose acetate system at  $25^\circ\text{C}$ .

spite the fact that the  $s$  and  $t$  values used in Eq. (9) are those obtained at  $170^\circ\text{C}$ . In nearly all systems studied in Ref. 12, the experimental values of  $f_{ce}$  are less than the calculated ones, but this is not the case here. There is no obvious explanation to this phenomenon, which appears to be due to contributions from  $\sigma(f)$  and  $\epsilon(f)$  unaccounted for in most percolation systems. Another example of behavior not expected from Refs. 1 and 2 is the frequency dependence of  $s$ , below  $\phi_c$ .<sup>12</sup>

$Z'-Z''$  and  $M'-M''$  (Cole-Cole) plots were made for all samples at both  $25$  and  $170^\circ\text{C}$ , as well as some intermediate temperatures, and carefully examined. The  $Z'-Z''$  plots gave depressed semicircular arcs, as is observed for effective media.<sup>16,17,24</sup> At  $25^\circ\text{C}$ , the only “single” arc that could be observed below  $\phi_c$  was that due to the magnetite, as the conductivity of the CA was too low for an impedance arc to be measured. Below  $\phi_c$ , at  $170^\circ\text{C}$ , the single impedance arc observed was that due to the CA, as the conductivity of the magnetite (actually conducting clusters) was now too high for an impedance arc to be measured successfully. Above  $\phi_c$ , the peaks of the single arc  $Z'-Z''$  results (not shown) give similar  $f_{cp}$  values to those given in Table II. However, the  $M'-M''$  plots were unexpectedly complex and, at first, incomprehensible. As the understanding of these plots is best obtained from  $M''$  against  $f$  together with  $Z''$  against  $f$  plots, these are what are presented below.

Figures 12 and 13 show the experimental results for  $Z''$  against  $f$  at  $25$  and  $170^\circ\text{C}$ , respectively, for samples above and below  $\phi_c$ . Figures 14 and 15 show simulated  $Z''(f)$  results at the two temperatures. Both the method and the parameters used to get the results will be given later. Figures 16 and 17 show the experimental results for  $M''$  against  $f$  at  $25$  and  $170^\circ\text{C}$ , respectively, while Figs. 18 and 19 show the simulated results at the two temperatures. It can be seen that the simulations, in Figs. 14, 15, 18, and 19, show semiquantitative agreement with the experimental results given in Figs. 12, 13, 16, and 17.

To enable the results, given in Figs. 12–19, to be more

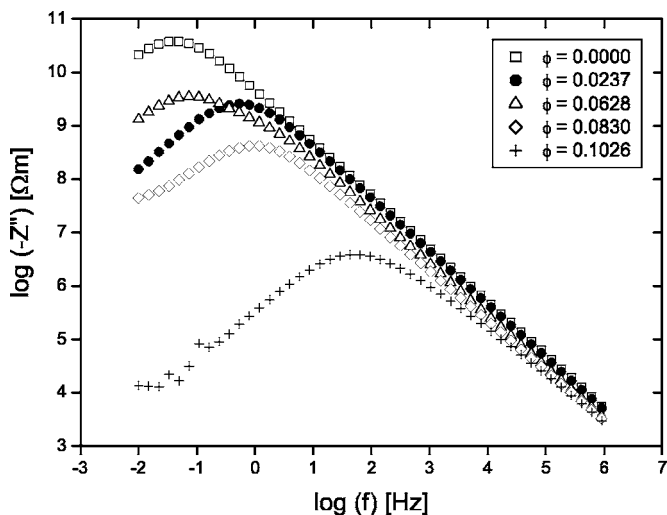


FIG. 13. Logarithm of imaginary impedance results plotted against logarithm of frequency for various samples of the  $\text{Fe}_3\text{O}_4$  in cellulose acetate system at  $170^\circ\text{C}$ .

easily understood, model simulations using Eq. (2) and ideal (nondispersive) components are given in Figs. 20 and 21. In these simulations, the model “nondispersive” insulating and conducting components have dc conductivities that are the same as those determined from fitting the  $170^\circ\text{C}$  CA-magnetite system dc results (Table I). An  $\epsilon_{ir}$  of 4.5 and an  $\epsilon_{cr}$  of 10 are used for the insulating and the more conducting component, respectively. The other parameters,  $\phi_c=0.085$ ,  $s=0.88$ , and  $t=5.33$ , are also within the error ranges of the  $170^\circ\text{C}$  CA-magnetite system dc values, given in Table I. The choice of the  $\phi_c$ ,  $s$ , and  $t$  values used in the simulations will become clearer later. Figures 20 and 21 show simulated plots of  $Z''$  and  $M''$  against frequency for  $\phi=0.0$  (pure insu-

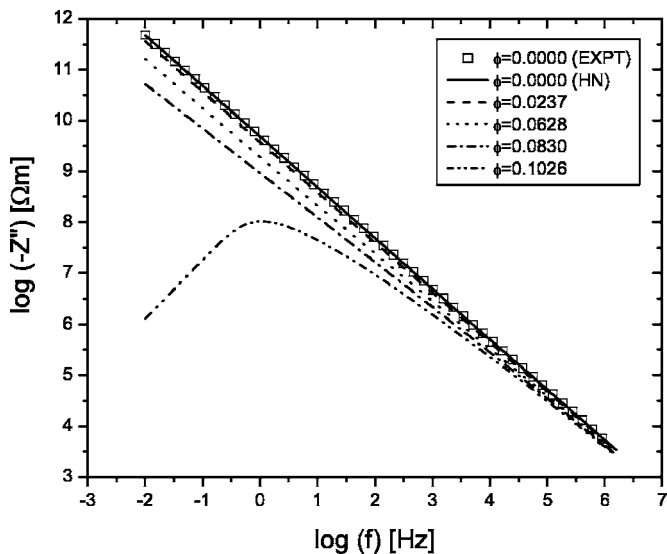


FIG. 14. Simulated results for imaginary impedance versus frequency for various samples at  $25^\circ\text{C}$  for the  $\text{Fe}_3\text{O}_4$  in cellulose acetate system. The simulation curves were obtained using the Havriliak-Negami equation and the TEPPE, with best-fit parameters, as described later.

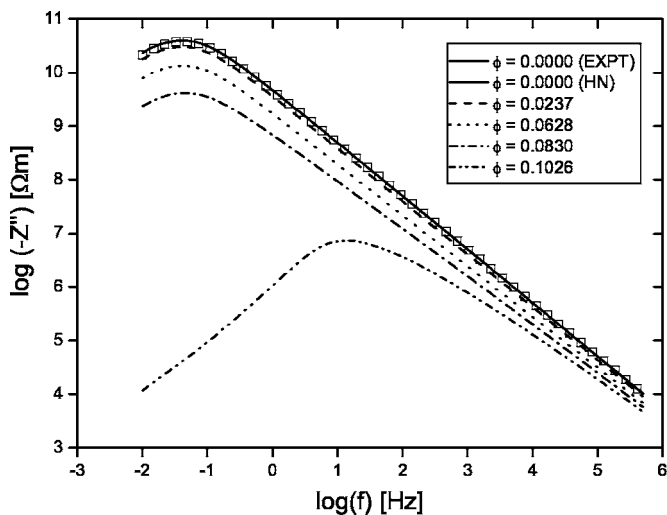


FIG. 15. Simulated results for imaginary impedance versus frequency for various samples at  $170^\circ\text{C}$  for the  $\text{Fe}_3\text{O}_4$  in cellulose acetate system. The simulation curves were obtained using the Havriliak-Negami equation and the TEPPE, with best-fit parameters, as described later.

lator), 0.0237, 0.0628, 0.0850 ( $\phi_c$ ), 0.1026, 0.5754, and 1.0 (more conducting component). The highest point of each plot is normalized to 1, which allows one to see the positions and shapes of peaks which have very different magnitudes. In Fig. 20, the  $Z''$  peak position remains fairly constant below  $\phi_c$ , which is consistent with the arcs observed in Fig. 13. Above  $\phi_c$ , the peak value of the single observable arc moves toward that of the more conducting component. In Fig. 21, the position of the low-frequency modulus ( $M''$ ) peak remains fairly constant below  $\phi_c$  and small high-frequency peaks (i.e., there are double peaks) start to appear even for  $\phi=0.0237$ . Just above  $\phi_c$ , the amplitude of the low-frequency peak rapidly drops when compared with the growing new high-frequency peak and vanishes for  $\phi$  values of about 0.1. This means that for percolation systems, there are

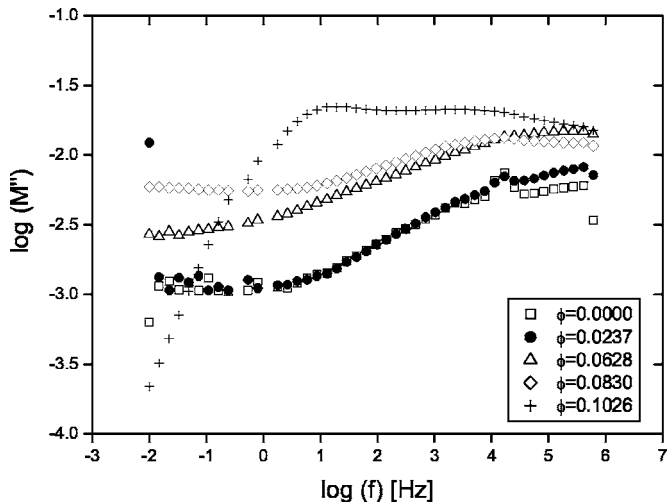


FIG. 16. Logarithm of imaginary modulus results plotted against logarithm of frequency for various samples of the  $\text{Fe}_3\text{O}_4$  in cellulose acetate system at  $25^\circ\text{C}$ .

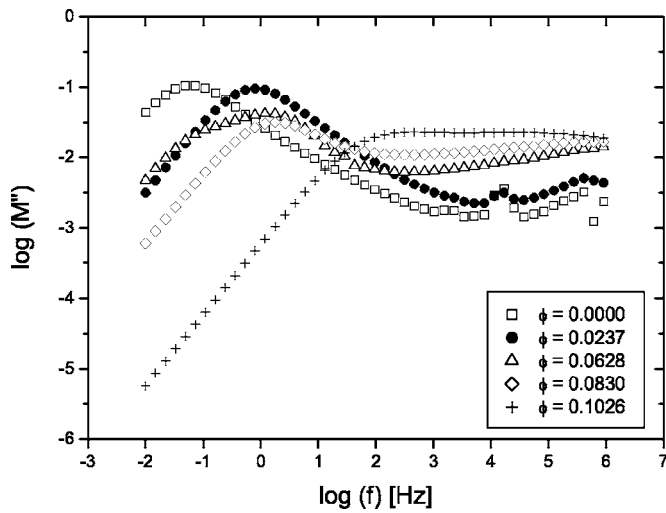


FIG. 17. Logarithm of imaginary modulus results plotted against logarithm of frequency for various samples of the  $\text{Fe}_3\text{O}_4$  in cellulose acetate system at  $170^\circ\text{C}$ .

still observable double peaks just above  $\phi_c$ . Note that the high-frequency peak frequencies stay fairly constant up to  $\phi_c$ . Above  $\phi_c$ , the peak frequencies increase toward the conducting component value ( $\phi=1.0$ ). Below  $\phi_c$ , these  $M''(f)$  peaks can only be due to the isolated conducting clusters, which appear to have a reasonably constant conductivity. This is followed by the contribution from the first spanning cluster at  $\phi_c$ . As  $\phi$  increases and the clusters continue to grow above  $\phi_c$ , their conductivity and peak frequencies increase, reaching that of magnetite at  $\phi=1$ . Note that at and close to  $\phi_c$  (i.e., the crossover region), there are similar contributions from both components to  $M''$ . Contributions from both components (i.e., double arcs) continue to be observed for samples just above  $\phi_c$ . This is in contrast to effective

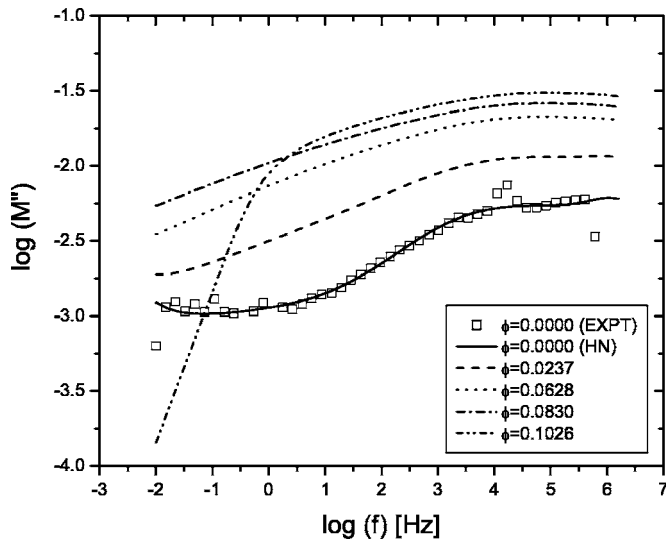


FIG. 18. Simulated results for imaginary modulus versus frequency for various samples at  $25^\circ\text{C}$  for the  $\text{Fe}_3\text{O}_4$  in cellulose acetate system. The simulation curves were obtained using the Havriliak-Negami equation and the TEPPE, with best-fit parameters, as described later.

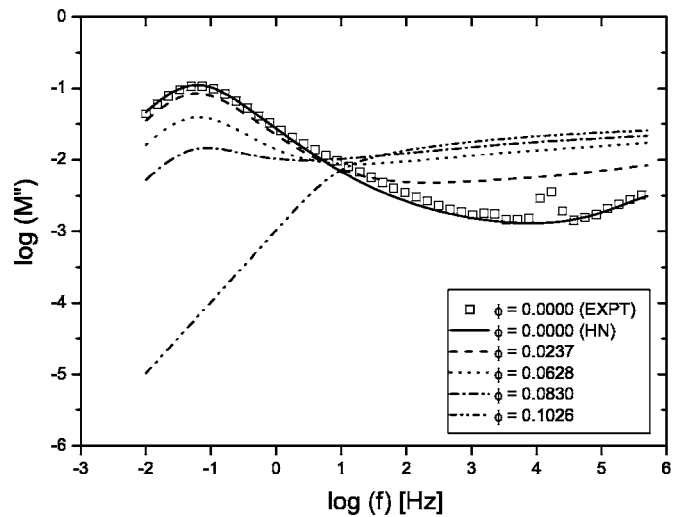


FIG. 19. Simulated results for imaginary modulus versus frequency for various samples at  $170^\circ\text{C}$  for the  $\text{Fe}_3\text{O}_4$  in cellulose acetate system. The simulation curves were obtained using the Havriliak-Negami equation and the TEPPE, with best-fit parameters, as described later.

media systems,<sup>16,17,24</sup> where two arcs, characteristic of each component, are observed when the insulating component surrounds, or coats, the conducting one, and a single arc, the peak frequency of which depends on  $\phi$ , is observed when the conducting component surrounds the insulating one. The corresponding plots at  $25^\circ\text{C}$  are not shown as the phenomena described above are not as clearly illustrated.

Following a better understanding of the  $Z''(f)$  and  $M''(f)$  spectra, the results in Figs. 14 and 15 and Figs. 18 and 19 were modeled as follows. First, the experimental results for the pure cellulose acetate, at  $25$  and  $170^\circ\text{C}$ , were fitted to the Havriliak-Negami equation, which is:<sup>25-27</sup>

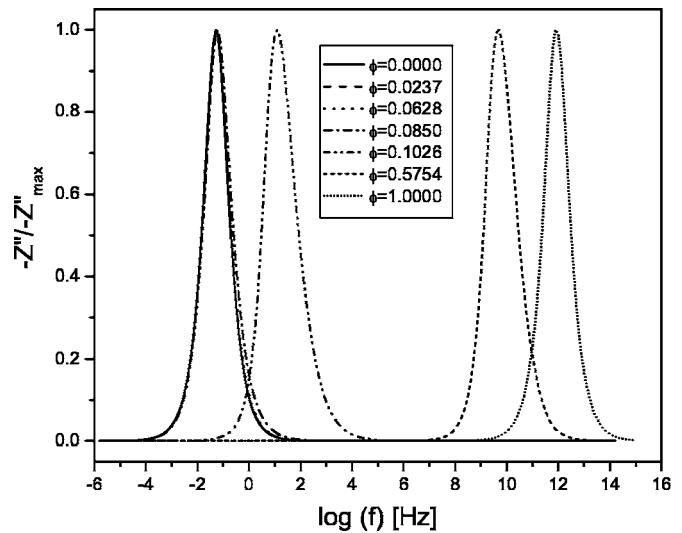


FIG. 20. Simulation results of the imaginary impedance versus frequency for various composites with different  $\phi$ 's. The simulation curves were obtained using the TEPPE with a simple conductivity model that assumes nondispersive materials for the insulating and conducting components.  $\phi_c=0.0850$ .

TABLE III. Best-fit parameters for the Havriliak-Negami expression for  $s=1$ .

Parameter	25 °C	170 °C
$\sigma(0)$ [ $(\Omega \text{ m})^{-1}$ ]	$2.83 \times 10^{-15}$	$1.08 \times 10^{-11}$
$\alpha_1$	0.167	0.943
$\beta_1$	1.000	0.558
$\epsilon_{\infty 1}$	1.460	0.694
$\Delta\epsilon_1$	0.210	2.310
$\tau_1$ (s)	0.332	10.270
$\alpha_2$	0.520	0.105
$\beta_2$	0.204	0.812
$\epsilon_{\infty 2}$	1.490	2.610
$\Delta\epsilon_2$	0.602	0.407
$\tau_2$ (s)	$1.24 \times 10^{-4}$	1.220
$\alpha_3$	1.000	0.782
$\beta_3$	0.702	0.803
$\epsilon_{\infty 3}$	0.0612	$1.82 \times 10^{-11}$
$\Delta\epsilon_3$	0.0417	0.0977
$\tau_3$ (s)	$1.60 \times 10^{-7}$	$1.46 \times 10^{-7}$

$$\epsilon^*(\omega) = \epsilon_r - i\epsilon_i = -i \left( \frac{\sigma(0)}{\omega\epsilon_0} \right)^n + \sum_{k=1}^3 \left[ \frac{\Delta\epsilon_k}{[1 + (i\omega\tau_k)^{\alpha_k}]^{\beta_k}} + \epsilon_{\infty k} \right], \quad 0 \leq \alpha, \beta, \quad n \leq 1,$$

$$\sigma^*(\omega) = \omega\epsilon_0\epsilon^*(\omega), \quad (13)$$

where  $\sigma(0)$  is the dc conductivity,  $k$  is the number of the particular relaxation process (maximum of 3), and  $\Delta\epsilon_k$  is the

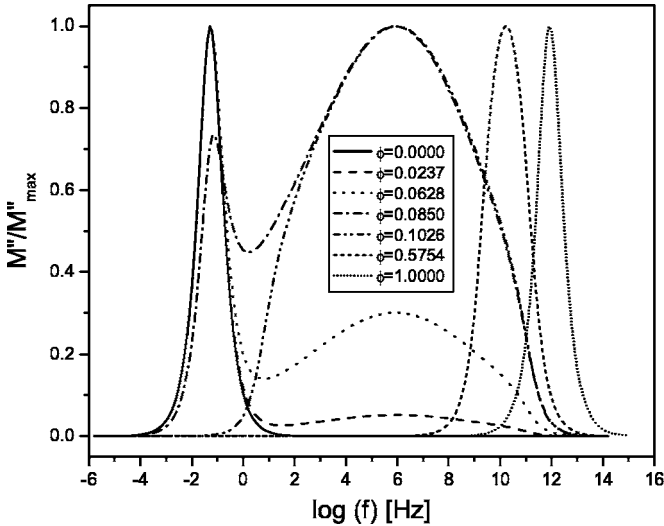


FIG. 21. Simulation results of the imaginary modulus versus frequency for various composites with different  $\phi$ 's. The simulation curves were obtained using the TEPPE with a simple conductivity model that assumes nondispersive materials for the insulating and conducting components.  $\phi_c=0.0850$ .

TABLE IV. Peak frequencies obtained from modulus and impedance plots for  $\phi=0.0830$ .

Temperature (°C)	$f_{\max}(M'')$ (Hz)	$f_{\max}(Z'')$ (Hz)	$f_{\max}(M'')/f_{\max}(Z'')$
120	0.0461	0.0270	1.707
140	0.2175	0.1104	1.970
160	0.9247	0.6460	1.431
170	2.6841	1.1882	2.259

difference in  $\epsilon_r$  at very low and at high frequencies for each relaxation process. The value of  $\epsilon_r$  at very high frequencies is  $\epsilon_{\infty}$ .  $\tau_k$  is the relaxation time,  $\alpha_k$  specifies the slope of the low-frequency side of the relaxation in  $\epsilon_i$ , and  $\beta_k$  is the asymmetry parameter for each process.<sup>26</sup> This is the only expression that allows one to model a high-frequency slope  $u_e$  greater than 1, as observed for the CA, and the best-fit parameters are given in Table III. The simulations were done by inserting the Havriliak-Negami expression, using the best-fit 25 °C parameters, for  $\sigma_i^*$ , together with the following other parameters into the TEPPE:  $\phi_c=0.085$ ,  $\epsilon_{cr}=10$ ,  $\sigma_{cr}=0.00269$  ( $\Omega \text{ cm})^{-1}$ ,  $t=4.57$ , and  $s=0.88$ . At 170 °C, the best-fit Havriliak-Negami expression for  $\sigma_i^*$  and the following other parameters are inserted into the TEPPE:  $\phi_c=0.085$ ,  $\epsilon_{cr}=10$ ,  $\sigma_{cr}=0.753$  ( $\Omega \text{ cm})^{-1}$ ,  $t=5.33$ , and  $s=0.88$ . All the above parameter values are within the error ranges of the dc fit. Note that some have been varied slightly, from the dc values, to better approximate the ac experimental results. In particular, a value of  $\phi_c=0.085$ , at the edge of the range permitted by the error in the dc results, is used. It can be seen in Figs. 12, 14, and 15 that between  $\phi=0.0830$  and 0.1026, the shapes of the  $Z''$  and  $M''$  curves change significantly and further ac simulations, with various values of  $\phi_c$ , showed that this change in shape occurs just above  $\phi_c$ , for any choice of the value of  $\phi_c$ . The shapes of the curves for the  $\phi=0.0830$  CA-magnetite indicate that it is below  $\phi_c$ . The value of  $\phi_c=0.0850$  was thus chosen for consistency of the

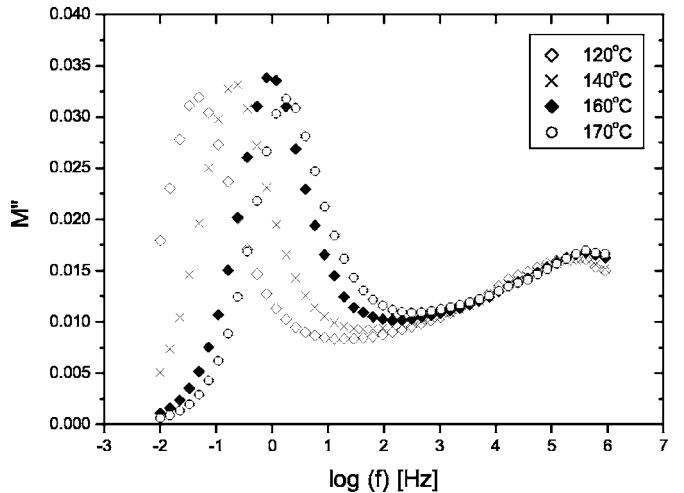


FIG. 22. Imaginary modulus plotted against logarithm of frequency at various temperatures for a  $\text{Fe}_3\text{O}_4$  in cellulose acetate sample ( $\phi=0.0830$ ) just above  $\phi_c$ .

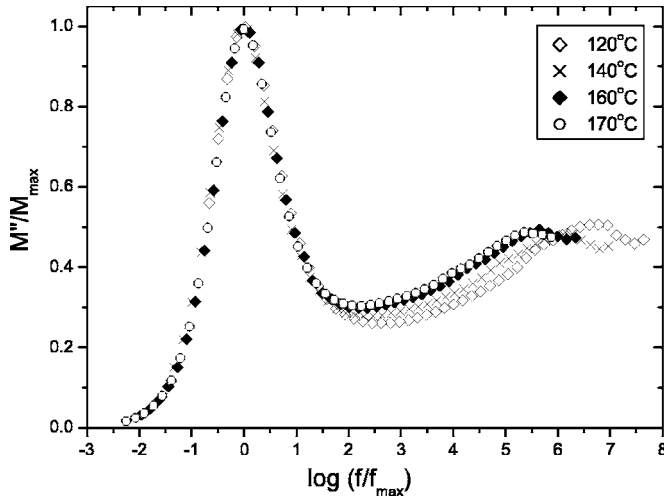


FIG. 23. Scaled imaginary modulus plotted against normalized frequency at various temperatures for the low-frequency peak of a  $\text{Fe}_3\text{O}_4$  in cellulose acetate sample ( $\phi=0.0830$ ), just above  $\phi_c$ .  $f_{\max}$  values are given in Table IV.

ac and dc results. A comparison between Figs. 12–15 as well as between Figs. 16–19 shows semiquantitative agreement.

Recently, work on some  $\text{NaNO}_3\text{-Al}_2\text{O}_3$  composites<sup>18</sup> plotted the imaginary modulus [ $M''(f)$ ] as a function of frequency, for the same sample, in order to investigate the shift in the peak frequency with temperature as well as to try and gain more insight into the behavior of the material under study. Scaling behavior was observed in the plots of the normalized modulus versus frequency. Similar plots (Figs. 22 and 23) have been made for a  $\text{Fe}_3\text{O}_4$ -CA sample, just above  $\phi_c$ , which show clearly the existence of two peaks, one low-frequency [corresponding to the dielectric material (CA)] and a rather smaller incomplete high-frequency magnetite and/or cluster peak. Figure 23 shows good scaling behavior, similar to that in Ref. 18 at the low-frequency modulus peak (see Table IV for the normalizing frequency values used in the scaling plot). However, an attempt to scale the results

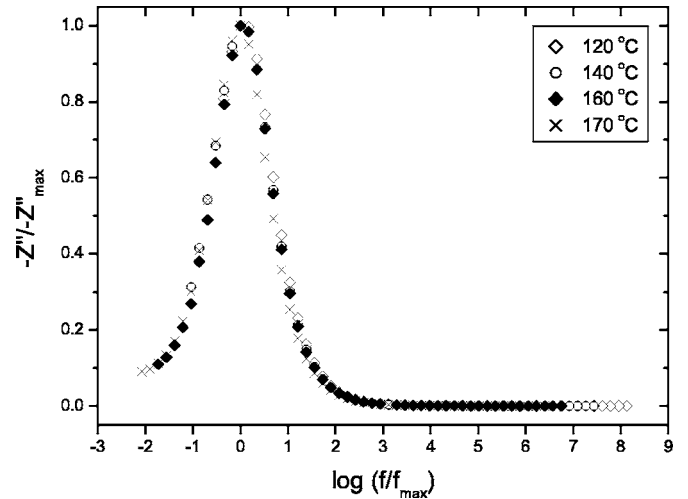


FIG. 25. Scaled imaginary impedance plotted against normalized frequency at various temperatures for the low-frequency peak of a  $\text{Fe}_3\text{O}_4$  in cellulose acetate sample ( $\phi=0.0830$ ) just above  $\phi_c$ .  $f_{\max}$  values are given in Table IV.

around the high-frequency peak did not yield satisfactory results. Plots of  $\log(Z'')$  against frequency, for the same sample at the same temperatures, were also made and are shown in Fig. 24. In this case, a logarithmic scale on the  $Z''$  axis is necessary because, unlike in the  $M''$  plots, the amplitude varies strongly with temperature. The corresponding normalized scaling plot for  $Z''$  (Fig. 25) shows that the overlap of the scaled curves is as good as that for  $M''$ . The corresponding peak frequencies are also given in Table IV. Note that the  $f_{\max}$  values for  $Z''$  are about one-half of those for the  $M''$  plots. No scaling of  $Z''(f)$  results is reported in Ref. 18. These results show that temperature scaling can be achieved in percolating systems, but these observations still require further experimental evidence and theoretical modeling especially as, in the present system, this form of scaling only works at and above 120 °C.

## V. CONCLUSIONS

The results presented in this paper show that the dc results are not affected by the use of a poor dielectric, i.e., a poor insulator at zero frequency, and that the two exponent phenomenological percolation equation can fit the results for a relatively high  $\sigma_{ir}/\sigma_{cr}$  ratio. Scaling of the dc results by varying the temperature [ $\sigma_{ir}(T)/\sigma_{cr}(T)$ ] is achieved and the results are universal in that the dc parameters can be used and  $u_e = u_i = t/(s+t)$ . Satisfactory scaling of the ac conductivity results,  $\log(\sigma_{mr}(\phi, f)/\sigma_{mr}(\phi, 0))$  against  $\log(f/f_{ce})$ , can be achieved by the usual sliding of the  $\sigma_{mr}(\phi, f)/\sigma_{mr}(\phi, 0)$  curves along the  $\log(\sigma_{mr}(\phi, f)/\sigma_{mr}(\phi, 0))=0$  line method to obtain the best empirical  $f_{ce}$  values. As impedance curves were measured in a percolation system, it was possible to discover that the peak frequency  $f_{cp}$ , obtained directly from the measured results of  $Z''(f)$ , could also be used as a satisfactory scaling frequency. The quality of the ac scaling definitely deteriorated as the dc conductivity of the CA started having an effect at 170 °C.

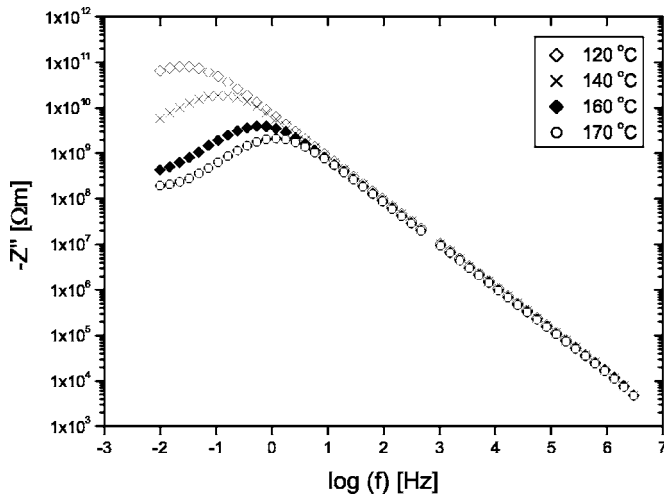


FIG. 24. Imaginary impedance plotted against logarithm of frequency at various temperatures for a  $\text{Fe}_3\text{O}_4$  in cellulose acetate sample ( $\phi=0.0830$ ), just above  $\phi_c$ .

The  $Z''$  versus frequency results are rather featureless and dominated by the insulating component. Not much can be learned from these plots. However, the  $M''$  versus frequency shows that there is both a high- and a low-frequency component contributing to the results. Using the two exponent phenomenological percolation equation and ideal nondispersive components, one can understand the  $M''$  versus frequency results as being made up of contributions from the CA and the percolating (conducting) clusters of magnetite-CA, both below and above  $\phi_c$ . The two exponent phenom-

enological equation and the Havriliak-Negami equation can adequately model the complex results obtained for the cellulose acetate-magnetite system. No morphological equation, other than the TEPPE, can achieve this. The present results emphasize the need, where possible, to analyze both the impedance and modulus spectra when studying composite and other systems. They also show that double  $M''(f)$  arcs are observable in percolation systems below and just above  $\phi_c$ , something which had not previously been observed.

---

\*Present address: Advanced Materials Division, Mintek, Private Bag X3015, Randburg 2125, South Africa. Electronic address: cosmasc@mintek.co.za

- <sup>1</sup>J. P. Clerc, G. Giraud, J. M. Laugier, and J. M. Luck, *Adv. Phys.* **39**, 191 (1990).
- <sup>2</sup>D. J. Bergman and D. Stroud, *Solid State Phys.* **46**, 148 (1992).
- <sup>3</sup>J. Wu and D. S. McLachlan, *Phys. Rev. B* **56**, 1236 (1997).
- <sup>4</sup>J. Wu and D. S. McLachlan, *Phys. Rev. B* **58**, 14880 (1998).
- <sup>5</sup>D. S. McLachlan, *J. Electroceram.* **5**, 93 (2000).
- <sup>6</sup>D. S. McLachlan, C. Chiteme, W. D. Heiss, and J. Wu, *Physica B* **338**, 256 (2003).
- <sup>7</sup>D. S. McLachlan, C. Chiteme, W. D. Heiss, and J. Wu, *Physica B* **338**, 261 (2003).
- <sup>8</sup>R. P. Kusy, *J. Appl. Phys.* **48**, 5301 (1977).
- <sup>9</sup>D. S. McLachlan, M. Blaszkiewicz, and R. E. Newnham, *J. Am. Ceram. Soc.* **73**, 2187 (1990).
- <sup>10</sup>D. S. McLachlan, *Mater. Res. Soc. Symp. Proc.* **411**, 309 (1996).
- <sup>11</sup>D. S. McLachlan, R. Rosenbaum, A. Albers, G. Eytan, N. Grammatica, G. Hurvits, J. Pickup, and E. Zaken, *J. Phys.: Condens. Matter* **5**, 4829 (1993).
- <sup>12</sup>C. Chiteme and D. S. McLachlan, *Phys. Rev. B* **67**, 024206 (2003).
- <sup>13</sup>D. S. McLachlan, W. D. Heiss, C. Chiteme, and J. Wu, *Phys. Rev. B* **58**, 13558 (1998).
- <sup>14</sup>W. D. Heiss, D. S. McLachlan, and C. Chiteme, *Phys. Rev. B* **62**, 4196 (2000).
- <sup>15</sup>C. Chiteme and D. S. McLachlan (private communication).
- <sup>16</sup>*Impedance Spectroscopy Emphasizing Solid Materials*, edited by J. R. Macdonald (Wiley-Interscience, New York, 1987).
- <sup>17</sup>D. S. McLachlan, J. H. Hwang, and T. O. Mason, *J. Electroceram.* **5**, 37 (2000).
- <sup>18</sup>P. S. Anantha and K. Hariharan, *Mater. Sci. Eng., B* **121**, 12 (2005).
- <sup>19</sup>P. M. Kogut and J. P. Straley, *J. Phys. C* **12**, 2151 (1979).
- <sup>20</sup>C. Chiteme, D. S. McLachlan, and I. Balberg, *Phys. Rev. B* **67**, 024207 (2003).
- <sup>21</sup>G. S. Grest, I. Webman, S. A. Safran, and A. L. R. Bug, *Phys. Rev. A* **33**, 2842 (1986).
- <sup>22</sup>D. S. McLachlan, G. Sauti, and C. Chiteme (private communication).
- <sup>23</sup>A. K. Jonscher, *Dielectric Relaxation in Solids* (Chelsea Dielectrics, London, 1983).
- <sup>24</sup>G. Sauti, Ph.D. thesis, Physics, University of the Witwatersrand, 2005.
- <sup>25</sup>S. Havriliak and J. Negami, *J. Polym. Sci., Part C: Polym. Symp.* **14**, 99 (1966).
- <sup>26</sup>G. Schaumburg, *Dielectrics Newsletter* (1995), pp. 9–12.
- <sup>27</sup>A. Schönhals, *Novo-Dielectrics Newsletter* 1 (1998).